Calcium stabilizes the von Willebrand factor A2 domain by promoting refolding

Amy J. Xu and Timothy A. Springer[1]

Immune Disease Institute, Program in Cellular and Molecular Medicine, Children's Hospital Boston, and Department of Biological Chemistry and Molecular Pharmacology, Harvard Medical School, Boston, MA 02115

Contributed by Timothy A. Springer, December 22, 2011 (sent for review October 24, 2011)

Von Willebrand factor (VWF) is a large, multimeric plasma glycoprotein that critically mediates hemostasis at sites of vascular injury. Very large VWF multimers have the greatest thrombogenic activity, which is attenuated by cleavage in the A2 domain by the metalloproteinase ADAMTS13. ADAMTS13 proteolysis requires mechanical force to expose the scissile bond and is regulated by a calcium-binding site within A2. In this study, we characterized the interaction between VWF A2 and calcium by examining the effect of calcium on VWF A2 stability and mechanical unfolding and refolding. Isothermal calorimetry yielded a calcium binding $K_d = 3.8 \pm 1.0\ \mu M$ and reversible thermal denaturation showed that 5 mM calcium stabilized the unfolding transition from 56.7 ± 0.1 to 69.1 ± 0.1 °C. Using optical tweezers to apply tensile force to single domains, we found that calcium did not affect VWF A2 unfolding, but rather enhanced refolding kinetics fivefold, resulting in a 0.9 kcal/mol stabilization in the folding activation energy in the presence of calcium. Taken together, our data demonstrate that VWF binds calcium at physiologic calcium concentrations and that calcium stabilizes VWF A2 by accelerating refolding.

Von Willebrand factor (VWF) is a large plasma glycoprotein that critically mediates hemostasis at sites of vascular injury. Secreted by endothelial cells and platelets in response to thrombogenic stimuli, VWF circulates as ultralong, disulfide-bonded concatamers (1) reaching >12 MDa and >15 μm in size (2, 3). Each VWF monomer is comprised of multiple domains, including domains that bind clotting factor VIII, collagen, platelets, and integrins (1). The A2 domain contains a cleavage site recognized by the enzyme ADAMTS13 (a disintegrin and metalloprotease with a thrombospondin type 1 motif, member 13), which regulates VWF length. The largest VWF concatamers mediate the formation of a platelet plug through multivalent binding to collagen and platelet membrane glycoprotein Ib. Mutations within VWF cause von Willebrand's disease (VWD), a heterogeneous set of bleeding disorders that underscore VWF function in normal physiology (4).

VWF function is critically determined by concatamer length. Healthy individuals exhibit a heterogeneous distribution of VWF concatamers, whose size is regulated through specific cleavage by ADAMTS13. Absence of ADAMTS13 function causes thrombocytic thrombocytopenic purpura (TTP), a life-threatening condition characterized by extensive microvascular thromboses that result in tissue ischemia and infarction. Neurologic symptoms and renal failure are often described, and the condition resolves upon replenishment of ADAMTS13 with plasma exchange (5). In contrast, genetic mutations that shift the VWF size distribution to smaller multimers, comprising type 2 VWD, present with increased bleeding due to reduced VWF thrombogenicity (6). Subtype 2A VWD mutations cluster within the A2 domain, which bears the ADAMTS13 cleavage site, and whose structure illuminates mechanisms that regulate VWF cleavage (7).

Fluid shear stress is critical for VWF size regulation (8) and VWF A2 is remarkable for several structural features that render the domain sensitive to hydrodynamic forces exerted on VWF concatamers in the circulation. The ADAMTS13 scissile bond is buried in a central β4-strand within A2 that is inaccessible in the native state (Fig. 1*A*). Compared to neighboring domains, VWF A2 lacks a long-range disulfide bond to protect the domain against unfolding by elongational (tensile) force exerted on VWF concatamers. Single molecule studies have demonstrated that ADAMTS13 cleavage requires unfolding of the A2 domain (7, 9) to expose the scissile bond. Furthermore, in place of an α4-helix, VWF A2 contains an "α4-less" loop that is thought to slow refolding to promote cleavage site accessibility (7). Thus, structural specializations within VWF A2 predict that reversible unfolding and refolding regulate VWF cleavage via dynamic accessibility of a buried scissile bond.

Recent studies have described a calcium-binding site that is unique amongst VWF A domains, and likely another structural specialization that regulates VWF A2 force sensing. VWF coordinates calcium by four residues from the α3-β4 loop and a single residue from the N-terminal β1-strand (10, 11) (Fig. 1*B*). Calcium binding was not seen in an earlier structure due to a lattice contact that enforced a conformation of the α3-β4 loop that precluded calcium binding (7, 10). Unfolding of A2 is predicted to proceed from the C terminus because, whereas the N-terminal β1-strand is clamped by hydrogen bonds in the center of the β-sheet, the C-terminal α6-helix is exposed and only locally hydrogen bonded (Fig. 1*A*). Furthermore, unfolding from the C terminus of secondary structure elements in the sequence of α6, β6, α5, β5, α4-less loop, and β4 exposes the minimal portion of the A2 domain required for maximal ADAMTS13 cleavage, as shown in peptide substrates (12). VWF A domains feature a "doubly wound" topology that juxtaposes two regions of sequentially arranged secondary structures. The α3-β4 loop lies at the junction between these two windings (Fig. 1*A*) and is thus in a strategic position to regulate A2 folding. In the sequential process of unfolding, the β4-strand bearing the scissile bond immediately precedes the α3-β4 loop. Cleavage assays of isolated A2 demonstrate that calcium binding protects the domain from cleavage by ADAMTS13 (10, 11), and protection against unfolding has also been reported (11). However, the quantitative details of how calcium stabilizes A2 remain to be defined.

In this study, we characterized the mechanisms underlying calcium stabilization of VWF A2. We derived thermodynamic parameters to quantitatively describe the interaction of calcium with VWF A2 and establish physiologic relevance. In parallel, we applied single molecule optical tweezers to functionally characterize the effect of calcium on A2 conformational dynamics. Combining such bulk and single molecule approaches, we gain a quantitative understanding of the conformational dynamics that regulate VWF cleavage.

Author contributions: A.J.X. and T.A.S. designed research; A.J.X. performed research; A.J.X. analyzed data; and A.J.X. and T.A.S. wrote the paper.

The authors declare no conflict of interest.

[1]To whom correspondence may be addressed at: Immune Disease Institute, Program in Cellular and Molecular Medicine at Children's Hospital Boston, 3 Blackfan Circle, Room 3103, Boston, MA 02115. E-mail: springer@idi.harvard.edu.

This article contains supporting information online at www.pnas.org/lookup/suppl/doi:10.1073/pnas.1121261109/-/DCSupplemental.

www.pnas.org/cgi/doi/10.1073/pnas.1121261109

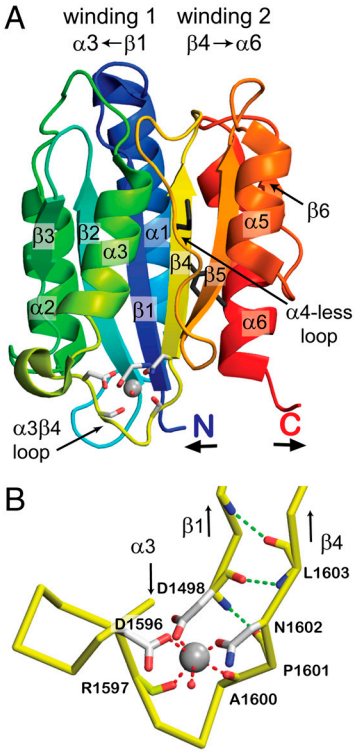

Fig. 1. VWF A2 structure. (*A*) A2 structural specializations. The scissile bond at Y1605/M1606 (gray sidechains) is buried within a central β4-strand. Elongational force experienced by VWF concatamers applied to the N and C termini renders A2 susceptible to ADAMTS13 cleavage. A calcium-binding site in the α3-β4 loop lies at the junction between windings 1 and 2, topologically defined by their sequential arrangements of secondary structures in opposite directions. (*B*) A2 calcium coordination. VWF A2 coordinates (red dashes) calcium (silver sphere) in octahedral geometry by six ligands, including a water molecule (small red sphere). Stabilizing hydrogen bonds are shown in green. The structure shown is a chimera containing residues 1495–1578 and 1602–1672 of 3GXB (9) and residues 1579–1601 of 3PPV (10). Figure made with PyMOL.

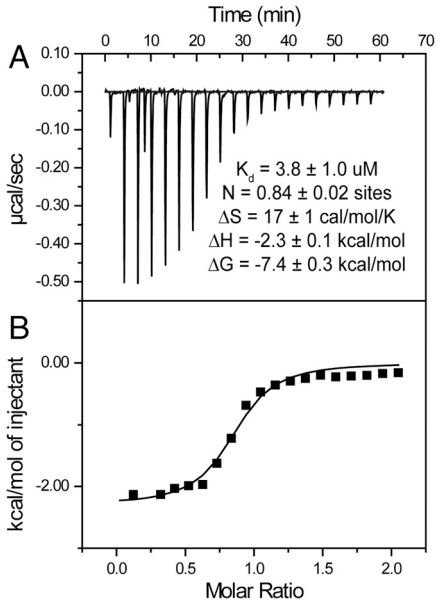

Fig. 2. Calcium-binding measurement by isothermal calorimetry. (*A*) Calorimetry. Reaction heats measured from stepwise calorimetry performed at 25 °C with 1.4 mM $CaCl_2$ injected against 140 μM A2 in the cell. (*B*) Binding isotherm. Calcium-binding affinity determined from calorimetry assuming single site binding.

Results

VWF A2 Binds Calcium with High Affinity. We employed isothermal calorimetry to determine the binding affinity of VWF A2 for calcium. Calcium was injected into a sample cell containing VWF A2 maintained at 25 °C. The A2 had been dialyzed against 5 mM EDTA, which was removed by gel filtration immediately before the experiment. The enthalpy of calcium binding monitored by measuring reaction heats after each calcium injection (Fig. 2*A*) was $\Delta H = -2.3 \pm 0.1$ kcal/mol. Binding of 0.84 mole calcium per mole of A2 suggested a single calcium-binding site within A2. Fitting the binding isotherms to a single binding site model (Fig. 2*B*) yielded $K_d = 3.8 \pm 1.0$ μM. The relationships $\Delta G = -RT\ln(1/K_d)$ and $\Delta S = (\Delta H - \Delta G)/T$ yield $\Delta G = -7.4 \pm 0.3$ kcal/mol and $\Delta S = 17 \pm 1$ cal/mol/K. Our results demonstrate that VWF A2 binds calcium with high affinity and that the free energy of the A2–calcium complex is substantially lower than that of its isolated components.

Calcium Stabilizes A2 in Native Conformation. To assess the effect of calcium on VWF A2 thermodynamic stability, we obtained CD spectra to monitor changes in secondary structure. At 4 °C, the CD spectra exhibited two negative bands at 222 and 208 nm (Fig. 3*A*, squares), a characteristic alpha helical spectrum (13) consistent with the high alpha helical content of VWF A2. Upon thermal denaturation, the spectra at 90 °C lost alpha helical signature (Fig. 3*A*, triangles). Thermal denaturation changes were reversible. Cooling the protein back down to 4 °C restored the alpha helical spectrum (Fig. 3*A*, circles). Similar changes in the native and denatured spectra were obtained in the presence and absence of calcium.

Calcium stabilized the native state of the A2 domain against thermal denaturation, monitored at 222 nm over a stepwise increase in temperature under equilibrium conditions of 3 min per °C (Fig. 3*B*). In the absence of calcium, VWF A2 remained stable until 50 °C, with a midpoint melting temperature, $T_m = 56.7 \pm 0.1$ °C. Chelating calcium with 1 mM EDTA did not change this transition, whereas 5 mM calcium stabilized the transition by 12 °C ($T_m = 69.1 \pm 0.1$ °C, Fig. 3*B*). No change was observed between 30 and 150 mM NaCl. Increasing calcium from 2 to 5 mM slightly increased thermal stability by 1.3 ± 0.1 °C, consistent with predictions for a two-state equilibrium (14).

To estimate changes in Gibbs free energy, thermal melts were analyzed according to Greenfield (15). Taking the 4 °C and 90 °C spectra to reflect the folded and unfolded states, respectively, the ratio of folded to unfolded A2 was determined from the signal at 222 nm. Experiments performed in the absence and presence of calcium were independently fit to the Gibbs–Helmholtz equation of free energy (Fig. 3*C*; $R^2 = 0.99$). Extrapolating the fits to 25 °C yielded Gibbs free energies of folding of -3.6 ± 0.8 kcal/mol in 5 mM calcium and -2.3 ± 0.1 kcal/mol in the absence of calcium.

Calcium Does Not Affect VWF Unfolding. We used optical tweezers to examine the effect of calcium on the mechanoregulation of A2 by tensile force. VWF A2 was covalently linked to DNA handles and suspended between two polystyrene beads, one anchored to the tip of a micropipette and another trapped within the infrared dual beam laser focus of the optical tweezers (Fig. 4*A*). Changes in light momentum reflected displacement, dx, of the bead from the center of the trap (Fig. 4*A*), and reported the force experienced by the protein–DNA tether with pN sensitivity. A2 unfolding was studied by monitoring force-extension profiles of single tethers (Fig. 4*B*).

To quantitatively characterize VWF A2 mechanoregulation, 1,881 pulls were analyzed under three experimental calcium conditions. A2 unfolding was reversible and robust (Fig. 4*C*) and the extension profiles of folded vs. unfolded constructs were well

BIOCHEMISTRY

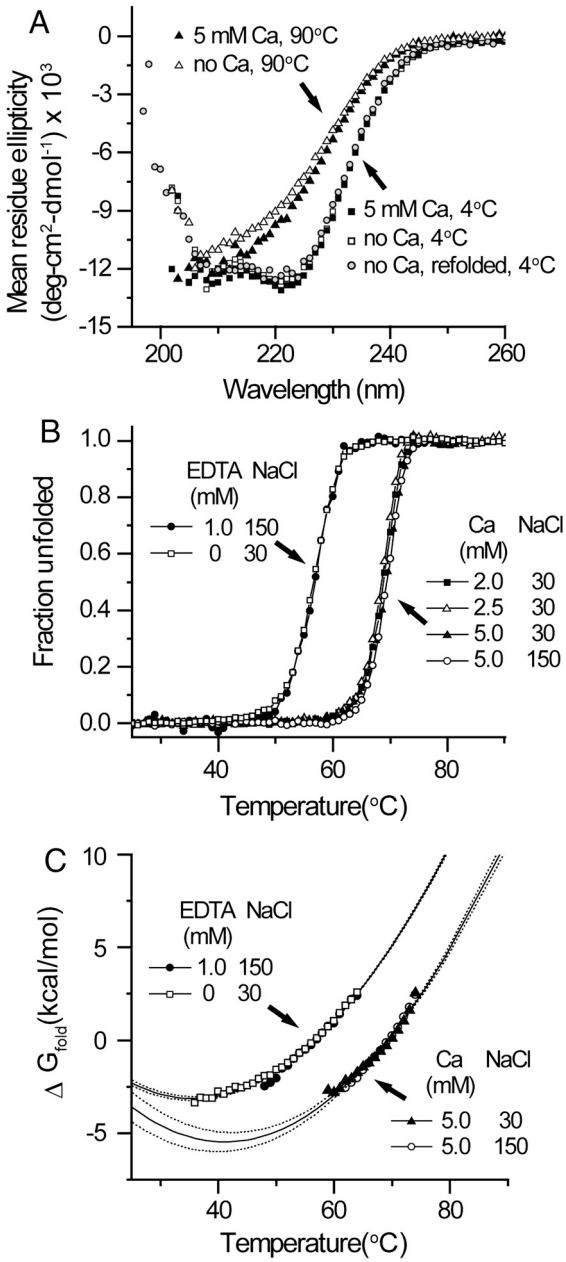

Fig. 3. Calcium stabilization of VWF A2 against thermal unfolding measured by CD. (*A*) CD spectra of VWF A2 in native and denatured states reflect α-helical content. Representative wavelength scans at 4 °C and 90 °C reflect secondary structure of VWF A2 in native (squares) and denatured (triangles) states, respectively. Structural changes are similar in the presence (filled symbols) and absence of calcium (open symbols) and are reversible (gray circles). (*B*) Calcium stabilizes VWF A2 against thermal denaturation. CD signal at 222 nm monitored over a stepwise increase in temperature at equilibrium (3 min per °C). (*C*) Calcium decreases free energy of VWF A2 protein folding. Thermal melts were analyzed according to Greenfield (15). Equilibrium data shown with fits to theory ($R^2 = 0.99$) and 95% confidence interval boundaries for free energy of protein folding.

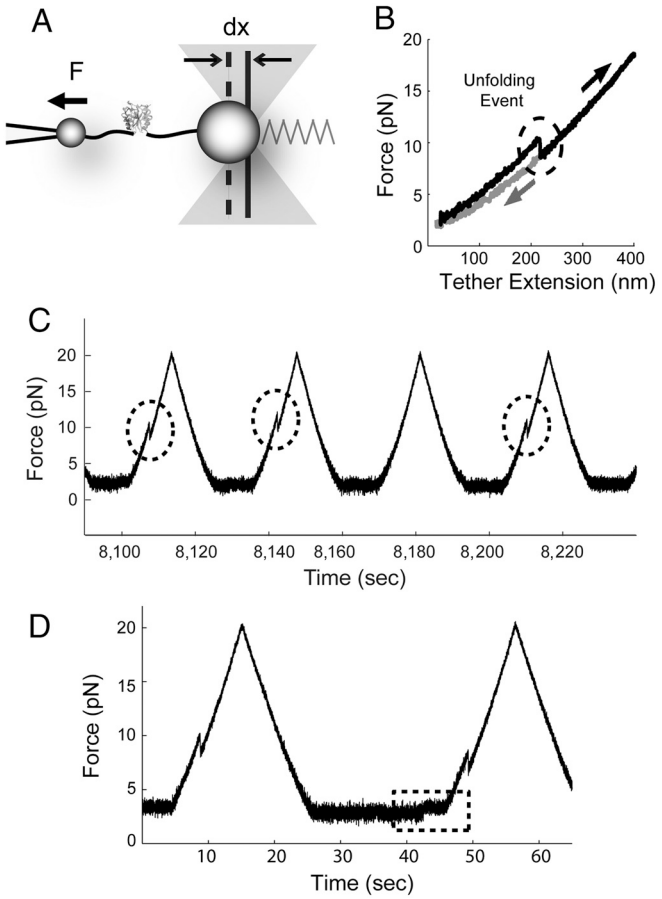

Fig. 4. Monitoring protein unfolding using optical tweezers. (*A*) Experimental setup. Force spectroscopy performed on single A2 domains suspended between two polystyrene beads by DNA handles. Excursions of the bead from the center of the trap reported the force experienced by the single molecule construct. (*B*) Force-extension profiles discriminate between unfolded and refolded constructs. Black trace follows ascent to 20 pN; gray curve follows relaxation to 2 pN. An abrupt force-extension discontinuity during the ascent resolves the force-extension profile of a folded vs. unfolded construct (circle). (*C*) A2 folding is reversible and robust. Representative pulling protocol: 40 nm/s pulling and relaxation rate (corresponding to force application rates of 0.5–2 pN/s) between 2 and 20 pN with 10 s pause at 2 pN. Force-extension discontinuities are highlighted. No unfolding is seen in the third pull of this trace but protein refolds before the subsequent fourth pull. (*D*) Direct visualization of refolding. When the trap was held at a constant position, giving a force of 3 pN prior to refolding, refolding was observed directly (dashed box) as a change to approximately 4 pN in force during the refolding pause cycle.

discriminated (Fig. 4*B*). In a representative trace, a folded construct was pulled at constant speed from 2 to 20 pN (Fig. 4*B*, black). At 14 pN, an abrupt discontinuity was observed with 37.4 nm extension (Fig. 4*B*, circle). Relaxation of the tether back down to the resting force (Fig. 4*B*, gray) retraced the force-extension profile of the unfolded construct. Once returned to a low force, tethers were held at constant position to allow refolding. At a moderate force of 3 pN, refolding was directly observed (Fig. 4*D*). However, at forces lower than 3 pN, the lower signal-to-noise ratio did not allow direct observations of refolding, and in most cases, refolding was measured indirectly from the presence or absence of unfolding in the subsequent pull (Fig. 4*C*).

Over a range of pulling rates, unfolding extensions displayed excellent agreement with full unfolding of VWF A2 when fit to the worm-like chain (WLC) model of polymer elasticity (Fig. 5 *A–D*). Single molecule data obtained in the absence of calcium (Fig. 5*A*), under calcium chelating conditions (1 mM EDTA, Fig. 5*B*), and in the presence of 5 mM Ca (Fig. 5*C*) yielded contour lengths, or lengths of maximum extension, of 76.3 ± 1.3 nm, 75.0 ± 1.6 nm, and 74.9 ± 1.3 nm, respectively. These results agreed with statistical significance within 4% ($p < 0.05$) and demonstrate that calcium does not affect mechanical extension of VWF A2 in the unfolded state. Fit to a global WLC model, the contour length was 75.6 ± 0.2 nm (Fig. 5*D*). In the crystal structure, the N-terminal and C-terminal residues Met1495 and Ser1671 are 1 nm apart

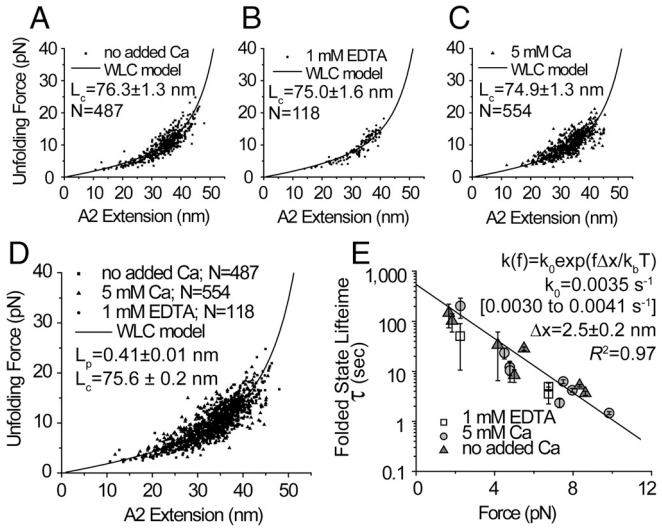

Fig. 5. Lack of effect of calcium on A2 unfolding. (*A–C*) Lack of effect of calcium on the increase in extension upon A2 unfolding. Independent WLC fits for data collected in the absence of calcium (*A*), in the presence of calcium (*B*), and under calcium chelating conditions (*C*) demonstrate that calcium does not affect A2 compliance in the unfolded state and that A2 exhibits full unfolding behavior under all three conditions. (*D*) Force-extension discontinuities from all experiments fit to a single WLC model. Individual fits agreed within 4% ($p < 0.05$). (*E*) Calcium does not affect kinetics of A2 unfolding. The force dependence of unfolding was derived from rupture-force histograms obtained over a range of pulling speeds according to the Hummer–Szabo–Dudko method (21). Errors shown are based on Poisson noise.

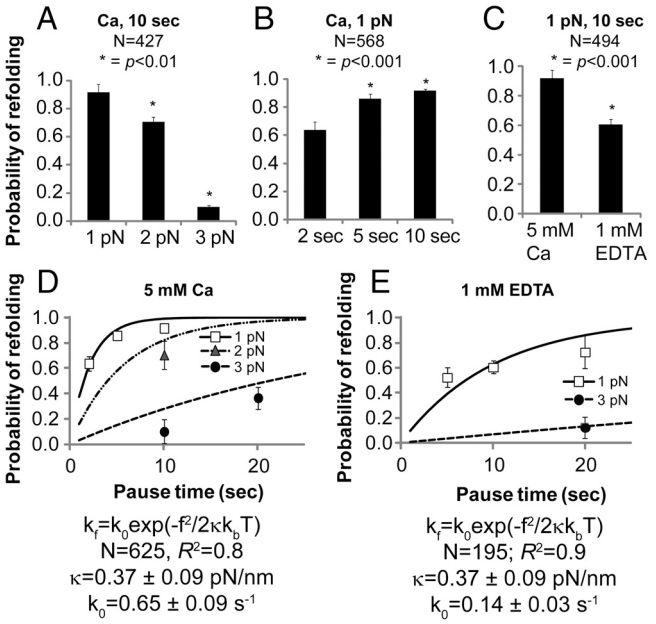

Fig. 6. Calcium enhances kinetics of VWF A2 refolding. (*A–C*) Binary refolding statistics demonstrate that probability of refolding was sensitive to force (*A*), time (*B*), and calcium (*C*). (*D–E*) Force dependence of refolding kinetics. Refolding probabilities fit to a single exponential dependence of refolding kinetics on the square of applied force (18).

(7). Thus, our data predict a 0.4 nm contour length per residue (75.6 + 1 = 76.6 nm divided by 177 residues), which agrees well with reported values (16), confirming the force-extension discontinuities observed as full A2 unfolding under all calcium conditions.

Unfolding kinetics were determined by examining the forces at which A2 unfolding was observed. The force dependence of unfolding was extracted from rupture-force histograms obtained over a range of pulling speeds (20–160 nm/s), corresponding to force application rates of 0.1–10 pN/s, according to the Dudko–Hummer–Szabo method (17). Data were fit to a single-barrier kinetic model, $k = k_0 \exp(f\Delta x/k_bT)$, where the unfolding rate is determined by the unfolding rate at zero force, k_0, and an exponential dependence on force, f, multiplied by the distance to the transition state, Δx (18). Fit independently, the intrinsic unfolding rates at zero force, k_0, were 0.0034 s^{-1} (95% confidence interval 0.0032 to 0.0037 s^{-1}) and 0.0036 s^{-1} (0.0032 to 0.0042 s^{-1}) in the presence and absence of calcium, respectively, agreeing with statistical significance within 20% ($p < 0.05$). A fit to all data in the presence and absence of calcium yielded $k_0 = 0.0035$ s^{-1} (0.0030 to 0.0041 s^{-1}) with a barrier to activation $\Delta x = 2.5 \pm 0.2$ nm ($R^2 = 0.97$, Fig. 5*E*).

Calcium Enhances VWF Refolding. Refolding kinetics were assessed by monitoring the probability of refolding across consecutive pulling cycles on the same construct (Fig. 4*C*). Single tethers were pulled then relaxed with loading rates of 0.1–10 pN/s. Once returned to a low force, the construct was held in constant position, corresponding to a constant force, to allow refolding (Fig. 4 *C* and *D*). Protein refolding was monitored by force-extension profiles (Fig. 4*B*) and the presence or absence of unfolding in a subsequent pull (Fig. 4*C*).

Observations of A2 refolding over many cycles ($N = 786$) demonstrated that A2 refolding was sensitive to force, time, and calcium. The probability of refolding significantly increased with decreased force (Fig. 6*A*) and increased time (Fig. 6*B*). Calcium chelation significantly decreased the probability of refolding (Fig. 6*C*). Both in the presence and absence of calcium, the kinetics of refolding, k_f, were well fit by a single exponential dependence on the refolding rate at zero force, k_0, the square of applied force, f^2, and the compliance of the unfolded state, κ (18) (Fig. 6 *D* and *E*). Under each calcium condition, data obtained at 1 pN, 2 pN, and 3 pN were globally fit to a single set of parameters. The intrinsic kinetics of refolding at zero force, k_0, in the presence and absence of calcium were 0.65 ± 0.09 s^{-1} and 0.14 ± 0.03 s^{-1}, respectively. This fivefold difference in refolding kinetics yields a 0.9 kcal/mol difference in the folding activation energy.

At moderate force, refolding was observed directly (Fig. 4*D*). In the presence of calcium at 3 pN, the lifetime of the unfolded state was 41 s (95% confidence interval 32 to 101 s, $N = 40$, 12 events observed directly), agreeing well with the unfolded state lifetime of 31 s expected from the kinetic model. In the absence of calcium, the 3 pN unfolded state lifetime was 96 s [(47 to 296 s), $N = 23$, five events observed directly], compared with 144 s predicted by the kinetic model. Thus, our direct observations of refolding agree well with the kinetic fits obtained from the much larger dataset of refolding probabilities.

Discussion

In this study, we report quantitative bulk measurements of calcium binding and folding thermodynamics, and single molecule measurements of unfolding and refolding kinetics, to understand the mechanisms underlying calcium stabilization of VWF A2 against cleavage. Isothermal calorimetry yielded a 3.8 μM binding affinity between A2 and calcium. The approximately 1.1–1.3 mM free calcium in healthy human blood is greatly above this measured K_d. Thus, the calcium-binding site is predicted to be saturated, establishing the relevance of calcium binding in VWF A2 under physiologic concentrations. Reversible thermal denaturation monitored using CD showed that calcium stabilized VWF A2 in the native state. We measured a thermodynamic stability shift of 12 °C in 5 mM calcium, which is consistent with the apparent 19 °C shift reported using fluorescent dye binding (11). Because our data were obtained under reversible conditions, we were able to estimate a folding free energy of −2.3 ± 0.1 kcal/mol in the absence of calcium and −3.6 ± 0.8 kcal/mol

in 5 mM calcium. The difference between these A2 unfolding energies predicts that 5 mM calcium stabilized the folded state by 1.3 ± 0.8 kcal/mol at 25 °C. Single molecule measurements of A2 unfolding and refolding demonstrated that calcium stabilizes A2 by promoting refolding. Unfolding measurements revealed that calcium had little if any effect on unfolding behavior. In contrast, calcium accelerated refolding approximately fivefold, lowering the activation barrier to refolding by 0.9 kcal/mol. Thus, we conclude that calcium stabilizes VWF A2 by promoting refolding.

Our thermodynamic and single molecule data allow us to postulate a free energy landscape for A2 unfolding (Fig. 7). Folding free energies determined by CD thermal denaturation indicate that native A2 (N) is stabilized by calcium (Fig. 7, gray). Similar unfolding kinetics in the presence and absence of calcium dictate similar activation energies from N to the unfolding transition state (TS 1). As a result, calcium stabilizes TS 1 to the same extent as N. Similar energetics are a consequence of similar structural environments (19). Thus, our results suggest that calcium occupies similar structural environments within TS 1 and N, indicating that TS 1 binds calcium with native-like coordination.

In the refolding direction, we assume that A2 does not bind calcium in the unfolded state (U), consistent with coordination of calcium by residues far apart in sequence (from residue 1498 to 1602) and with the similar contour lengths measured in the presence and absence of calcium (Fig. 5). Going from calcium-free U to calcium-bound N, the significant binding energy between calcium and A2 measured by isothermal calorimetry precludes the calcium-binding event from occurring during a transition state. Given that TS 1 binds calcium, such a calcium-free transition state in the refolding direction (TS 2) requires a calcium-binding intermediate (I). Indeed, an unfolding intermediate has been previously described at 1,000 Hz with a 1.2 ms lifetime (9), too transient to be characterized by our data acquired at 500 Hz but consistent with an intermediate structure with high energy relative to N and U (Fig. 7). Further insight into TS 2 is gleaned from the dependence of refolding on calcium. Our single molecule data demonstrate that calcium accelerates refolding. Thus, the rate-limiting transition state from calcium-free U to calcium-bound N must also bind calcium, and cannot be TS 2. Instead, TS 1 functions as the kinetically relevant transition state by occupying a higher energy level than TS 2 in the refolding pathway. In our model, the disparate effects of calcium on the unfolding and refolding kinetics are accounted for by an unfolding transition state, TS 1, that binds calcium with native-like coordination, and that is rate limiting in both unfolding and refolding pathways.

The known three-dimensional structure of A2 (Fig. 1) places some limits on the structure of calcium-binding TS 1. As previously introduced, calcium binds A2 at the junction between two topologically defined windings (Fig. 1*A*). Both windings begin near the center of the β-sheet but proceed in opposite directions.

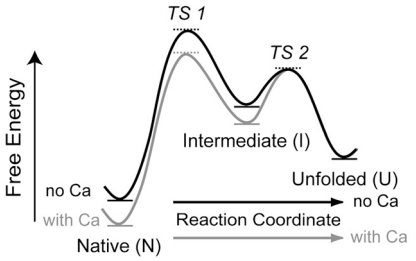

Fig. 7. Proposed A2 energy landscape. Our proposed free energy landscape describing calcium stabilization of A2 features a calcium-binding native state (N); a calcium-binding transition state (TS 1) that binds calcium with native-like coordination and is rate- imiting in both the unfolding and refolding directions; a high energy, calcium-binding intermediate (I); a calcium-free transition state (TS 2) in the refolding pathway; and a non-calcium-binding unfolded state (U).

Winding 1 proceeds from the central β1-strand to the α3-helix, whereas winding 2 proceeds from the central β4-strand to the α6-helix (Fig. 1*A*). The calcium-binding site includes Asp-1498 in the β1-strand, residues 1596, 1597, and 1600 in the α3-β4 loop, and Asn-1602 in the β4-strand (Fig. 1*B*). Similar unfolding kinetics implicate native-like coordination of calcium within the unfolding transition state and locate the boundary between native-like and unfolded regions of A2 between the β4-strand and the C terminus. This region includes the α4-less loop that, like the calcium-binding site, might be important in regulating the kinetics of A2 refolding. Such a model is also consistent with the idea that unpopping of the rigid C-terminal vicinal disulfide plug could be rate limiting for unfolding, as previously proposed (1).

A very recent study used optical tweezers to report that A2 unfolding requires higher forces in the presence of calcium and primarily proceeds through a mechanically stable intermediate (11). Force-extension behavior in this study was measured at 50 Hz and exhibited slow unfolding and refolding (on the order of seconds) with unfolding intermediates lasting 1–3 s. This behavior clearly differs from the highly cooperative unfolding and refolding (within milliseconds) previously reported (9) and observed in our study, as well as the 1.2 ms lifetimes previously reported for A2 unfolding intermediates (9). Because we did not observe such slow phenomena in our thousands of characterized events, we think it is unlikely that A2 follows an alternative unfolding pathway, but rather attribute these discrepancies to different methods for suspending single molecules of A2 between beads. Whereas we attached DNA handles to both ends of A2, holding A2 approximately 260 nm away from each bead and preventing nonspecific interactions, the other study attached DNA at only one end of the A2 construct. Their A2 N terminus contained a $(\text{c-myc})_4$ tag that directly bound an anti-c-myc antibody-coated bead, placing A2 approximately 840 nm away from the DNA-bound bead but only 0–30 nm away from the $(\text{c-myc})_4$ tag-bound bead [depending on whether the antibody coupled through its Fab or Fc region to the bead, which of the four c-myc tags the antibody (20) bound to, and fluctuations in the flexible c-myc tags and antibody at low force]. DNA handles are not only much longer but also much stiffer than the c-myc tags. We speculate that direct physisorption of the A2 protein to the anti-c-myc bead could have occurred, and that sequential force discontinuities summing to the overall contour length of the polypeptide could have been convoluted with A2 unfolding and refolding. Robustness of the 28 measured events (11) was not tested by fits to biophysical models that predict exponential dependence of unfolding and refolding rates on applied force (17, 21). In contrast, our 1,881 events were fit to such models, and we have reported estimates of k_0 and Δx for unfolding, and k_0 and κ for refolding.

VWF is a multidomain protein and interdomain interactions are likely important for regulating function. Thus, our study is limited in characterizing conformational dynamics within isolated VWF A2. However, studies on the A1-A2-A3 tridomain have demonstrated that force-induced A2 unfolding is required for cleavage in the presence of neighboring domains as well (22, 23), and that calcium mediated stabilization against thermal denaturation is exclusive to the A2 domain (11), affirming the relevance of understanding unfolding dynamics within the isolated A2 domain.

ADAMTS13 circulates in the body as a constitutively active enzyme, with cleavage regulated by conformational changes within its substrate, VWF. Much attention on A2 conformational regulation has focused exclusively on unfolding (22, 23). However, given the slow kinetics of refolding, at equilibrium, VWF A2 is predicted to be fully unfolded at forces above 5 pN (Fig. S1), significantly lower than the 10 pN peak force estimated to be experienced by a 200-mer VWF at the highest shear stress measured in arteriolar flow (9). The concentration of ADAMTS13 in vivo is estimated at 6 nM (24), well below the estimated K_m of 160 nM (9) required for saturation binding to its unfolded substrate.

Therefore, the time required for refolding regulates the availability of unfolded A2 for cleavage. Our data suggest that refolding plays a critical role in regulating VWF proteolysis and highlights the dynamic nature of A2 conformational change in dictating VWF function.

Materials and Methods

CD. CD spectra were obtained on an Aviv 62 DS spectropolarimeter equipped with a Peltier temperature control unit (Aviv Associates). A2 protein (2 μM) in 20 mM Tris (pH 7.50), 30 or 150 mM NaCl, and varying concentrations of EDTA or $CaCl_2$ was monitored within a 1.0 cm pathlength quartz cuvette with a magnetic stirrer. Baseline spectra of the folded and unfolded states were obtained at 4 °C and 90 °C, respectively, with five accumulations scanned from 260 to 195 nm at 1.0 nm intervals. Thermal denaturation was monitored at 222 nm from 4 to 90 °C at 1 °C intervals, equilibrating for 2 min at each temperature before signal averaging for 1 min. Spectra shown are corrected for background contribution of buffer. Thermal unfolding curves were derived from linear fits to thermal denaturation signal before and after the unfolding transition. Single wavelength CD temperature melts were fit to a Gibbs–Helmholtz equation as described by Greenfield (15).

Isothermal Calorimetry. Isothermal calorimetry was conducted on an iTC_{200} (Microcal) in a 200 μL reaction cell loaded with 140 μM protein at 25 °C. To ensure complete removal of calcium, protein was dialyzed for 3 d against 5 mM EDTA, which was then removed via gel filtration on a Superdex 75 10/300 column (GE Lifesciences) immediately before the experiment. Titration was performed using 20×2 μL injections of 1.4 mM $CaCl_2$ in the same buffer (20 mM Tris, pH 7.5, 30 mM NaCl) at 180 s intervals, stirring at 1,000 rpm. Binding isotherms were analyzed using the Microcal Origin version 7 software package and fit to a single site binding model.

Protein Expression and Purification. VWF A2 domain was prepared as previously described (9).

Single Molecule Sample Preparation. DNA handles (802 base pairs) were PCR-amplified using forward primers with a 5′thiol group and reverse primers with either 5′biotin or 5′digoxigenin and activated with 2,2′-dithio-dipyridine (DTDP) as described previously (9). For protein–DNA coupling, 50 μL of 12 μM protein was reduced with 1 mM DTT for 1 h at room temperature, followed by three sequential passages through 0.5 mL Zeba desalting columns (Pierce). Freshly reduced A2 (5 μM) was reacted with 3 μM DTDP activated handles in 20 μL 0.2 M sodium acetate (pH 5), 1 M NaCl, 1 mM EDTA. Reaction components were quickly mixed before incubating under argon in a 1.5 mL Eppendorf for 16 h at room temperature. In our hands, coupling was tricky and highly sensitive to DNA:protein ratios. Due to small volumes and rapid oxidation, precise concentrations were difficult to predict and thus coupling was performed in parallel across a range of DNA:protein ratios (Fig. S2*B*). Different handle preparations varied in coupling efficiency and the preparations were selected as described below and used for experiments. Coupling efficiency was assayed by running reaction products on 4–20% polyacrylamide gels. Ethidium bromide staining reported shifts in DNA handles upon successful coupling to A2, which was specifically verified via Western blot analysis on the same gel (Fig. S2*A*). As final verification, constructs were tested on single molecule optical tweezers. For constructs with poor coupling efficiency, only DNA handle dimers or nonspecific extension lengths were observed with great effort. Successful coupling yielded constructs with reliable observations of single A2 unfolding events (>50% of tethers). Verified DNA/protein coupled constructs were aliquoted and stored at −80 °C.

Single Molecule Force Experiments. Polystyrene beads (4.2 μm, Spherotech) functionalized with antidigoxigenin Fab (Roche) were incubated with 10 pM protein-DNA constructs for 30 min at room temperature (optimized for single tethers). Single beads were then trapped in the laser tweezers and brought close to a streptavidin-functionalized polystyrene bead (2.1 μm) suctioned onto the tip of a micropipette. Single tether formation was verified by overstretching the construct past 65 pN to confirm the signature force-extension curve plateau corresponding to the B to S form DNA transition (25). The average tether lasted 80 cycles with force-extension discontinuities observed in 75% of pulls. All pulls from each tether were used for analysis. The instrument used for optical trapping has been previously described (26). Experiments were conducted in 20 mM Tris (pH 7.5), 150 mM NaCl, 0.02% Tween 20. Experiments were conducted with no added calcium [buffer confirmed as <20 μM Ca via a QuantiChrom Calcium Assay Kit (Bioassay Systems)], with 5 mM $CaCl_2$, and with 1 mM EDTA.

Statistical Analysis. Errors are estimated errors based on χ^2 minimized fits using Origin 6.1 (OriginLab Corporation). Data were noted to be statistically similar by comparing the maximal spread of 95% confidence intervals.

ACKNOWLEDGMENTS. The authors thank Dr. S.C. Blacklow for isothermal calorimetry and CD equipment and advice. This work was supported by National Institutes of Health (NIH) HL-48675 (T.A.S.) and NIH/National Institute of General Medical Sciences T32 GM008313 Molecular Biophysics Training Grant (A.J.X.). A.J.X. is an MD/PhD candidate at Harvard Medical School and this work is submitted in partial fulfillment of the requirement for the PhD.

1. Springer TA (2011) Biology and physics of von Willebrand factor concatamers. *J Thromb Haemost* 9(Suppl 1):130–143.
2. Hoyer LW, Shainoff JR (1980) Factor VIII-related protein circulates in normal human plasma as high molecular weight multimers. *Blood* 55(6):1056–1059.
3. Schneider SW, et al. (2007) Shear-induced unfolding triggers adhesion of von Willebrand factor fibers. *Proc Natl Acad Sci USA* 104:7899–7903.
4. Sadler JE (2005) New concepts in von Willebrand disease. *Annu Rev Med* 56:173–191.
5. Sadler JE, Moake JL, Miyata T, George JN (2004) Recent advances in thrombotic thrombocytopenic purpura. *Hematology Am Soc Hematol Educ Program* 2004:407–423.
6. Sadler JE (2008) Von Willebrand factor, ADAMTS13, and thrombotic thrombocytopenic purpura. *Blood* 112:11–18.
7. Zhang Q, Zhou Y-F, Zhang C-Z, Springer TA (2009) Structural specializations of A2, a force-sensing domain in the ultralarge vascular protein von Willebrand factor. *Proc Natl Acad Sci USA* 106:9226–9231.
8. Dong JF, et al. (2002) ADAMTS-13 rapidly cleaves newly secreted ultralarge von Willebrand factor multimers on the endothelial surface under flowing conditions. *Blood* 100:4033–4039.
9. Zhang X, Halvorsen K, Zhang CZ, Wong WP, Springer TA (2009) Mechanoenzymatic cleavage of the ultralarge vascular protein, von Willebrand factor. *Science* 324:1330–1334.
10. Zhou M, et al. (2011) A novel calcium-binding site of von Willebrand factor A2 domain regulates its cleavage by ADAMTS13. *Blood* 117:4623–4631.
11. Jakobi AJ, Mashaghi A, Tans SJ, Huizinga EG (2011) Calcium modulates force sensing by the von Willebrand factor A2 domain. *Nat Commun* 2(385):1–9.
12. Cruz MA, Whitelock J, Dong JF (2003) Evaluation of ADAMTS-13 activity in plasma using recombinant von Willebrand factor A2 domain polypeptide as substrate. *J Thromb Haemost* 90(6):1204–1209.
13. Toumadje A, Alcorn SW, Johnson WC, Jr (1992) Extending CD spectra of proteins to 168 nm improves the analysis for secondary structures. *Anal Biochem* 200:321–331.
14. Boeckler FM, et al. (2008) Targeted rescue of a destabilized mutant of p53 by an in silico screened drug. *Proc Natl Acad Sci USA* 105:10360–10365.
15. Greenfield NJ (2006) Using circular dichroism collected as a function of temperature to determine the thermodynamics of protein unfolding and binding interactions. *Nat Protoc* 1:2527–2535.
16. Ainavarapu SR, et al. (2007) Contour length and refolding rate of a small protein controlled by engineered disulfide bonds. *Biophys J* 92:225–233.
17. Dudko OK, Hummer G, Szabo A (2006) Intrinsic rates and activation free energies from single-molecule pulling experiments. *Phys Rev Lett* 96:108101–108104.
18. Evans E, Ritchie K (1997) Dynamic strength of molecular adhesion bonds. *Biophys J* 72:1541–1555.
19. Daggett V, Li A, Itzhaki LS, Otzen DE, Fersht AR (1996) Structure of the transition state for folding of a protein derived from experiment and simulation. *J Mol Biol* 257(2):430–440.
20. Krauss N, et al. (2008) The structure of the anti-c-myc antibody 9E10 Fab fragment/epitope peptide complex reveals a novel binding mode dominated by the heavy chain hypervariable loops. *Proteins* 73:552–565.
21. Dudko OK, Hummer G, Szabo A (2008) Theory, analysis, and interpretation of single-molecule force spectroscopy experiments. *Proc Natl Acad Sci USA* 105:15755–15760.
22. Wu T, Lin J, Cruz MA, Dong JF, Zhu C (2010) Force-induced cleavage of single VWF A1A2A3-tridomains by ADAMTS-13. *Blood* 115:370–378.
23. Ying J, Ling Y, Westfield LA, Sadler JE, Shao JY (2010) Unfolding the A2 domain of von Willebrand factor with the optical trap. *Biophys J* 98:1685–1693.
24. Feys HB, et al. (2006) ADAMTS-13 plasma level determination uncovers antigen absence in acquired thrombotic thrombocytopenic purpura and ethnic differences. *J Thromb Haemost* 4:955–962.
25. Smith SB, Cui Y, Bustamante C (1996) Overstretching B-DNA: The elastic response of individual double-stranded and single-stranded DNA molecules. *Science* 271:795–799.
26. Kim J, Zhang C, Zhang X, Springer TA (2010) A mechanically stabilized receptor-ligand flex-bond important in the vasculature. *Nature* 466:992–995.